Supporting Information

A novel anion-pillared metal–organic framework for highly efficient separation of acetylene from ethylene and carbon dioxide

Quan-Li Qian[‡a], Xiao-Wen Gu[‡a], Jiyan Pei[a], Hui-Min Wen[b], Hui Wu[c], Wei Zhou*[c], Bin Li*[a], and Guodong Qian*[a]

[a] State Key Laboratory of Silicon Materials, Department of Materials Science & Engineering, Zhejiang University, Hangzhou 310027, China. E-mail: bin.li@zju.edu.cn; gdqian@zju.edu.cn

[b] College of Chemical Engineering, Zhejiang University of Technology, Hangzhou, 310014, China

[c] NIST Center for Neutron Research, National Institute of Standards and Technology, Gaithersburg, Maryland 20899-6102, United States. E-mail: wzhou@nist.gov

‡ These authors have contributed equally to this work.

Experimental Section

1. Powder X-Ray Crystallography. Attempts to obtain single crystals of ZJU-280 for single-crystal X-ray diffraction measurement were not successful. Thus powder X-ray diffraction (PXRD) was relied on to confirm high purity of the powder sample and to simulate the crystallographic structure.[1] The PXRD measurements were performed on an X'Pert PRO diffractometer, operated at 40 kV and 44 mA and Cu K_α radiation (λ= 1.542 Å). Data were collected in the 2θ range of 2-45º with a step size of 0.2º at room temperature. We first indexed the PXRD pattern and used a monoclinic *P2/m* space group to build the model of ZJU-280. Then, based on the similar 4-connercted framework of CPM-131,[2] a structural model for ZJU-280 was built. The pyridine groups were modeled as fully ordered in the structure and the orientation of pyridine rings was optimized. In reality, there may exist some orientational disorder associated with pyridine groups. As shown in Figure S2, the simulated PXRD pattern of our structural model agrees excellently with experimental data, strongly supporting its validity. Some structural information of ZJU-280 is given in Table S1.

2. Fitting of pure component isotherms

Experimental data on pure component isotherms for C_2H_2, CO_2 and C_2H_4 in ZJU-280a were measured at 273 K and 296 K. The pure component isotherm data for C_2H_2, CO_2 and C_2H_4 were fitted with Dual site Langmuir-Freundlich (DSLF) model.

$$N = N_1^{max}\frac{b_1 p^{1/n1}}{1 + b_1 p^{1/n1}} + N_2^{max}\frac{b_2 p^{1/n2}}{1 + b_2 p^{1/n2}} \quad (1)$$

Where N (unit: mol/kg) is the adsorbed amount per mass of adsorbent. N_1^{max} and N_2^{max} (unit: mol/kg) are the saturation capacities of site Ⅰ and site Ⅱ, p (unit: kPa) is the pressure of the bulk gas at equilibrium with the adsorbed phase. b_1 and b_2 (unit: $kPa^{-1/n}$) are the affinity coefficients of site Ⅰ and site Ⅱ, and n_1 and n_2 represent the deviation from an ideal homogeneous surface.

3. Viral Graph Analysis

Estimation of the isosteric heats of gas adsorption (Q_{st})

A virial-type expression of comprising the temperature-independent parameters a_i and b_j was employed to calculate the enthalpies of adsorption for C_2H_2, CO_2 and C_2H_4 (at 273 K and 296 K) on ZJU-280a. In each case, the data were fitted with equation:

$$\ln P = \ln N + 1/T \sum_{i=0}^{m} a_i N^i + \sum_{j=0}^{n} b_j N^j \qquad (2)$$

Here, P is the pressure expressed in Pa, N is the amount absorbed in mmol g^{-1}, T is the temperature in K, a_i and b_j are virial coefficients, and m, n represent the number of coefficients required to adequately describe the isotherms (m and n were gradually increased till the contribution of extra added a and b coefficients were deemed to be statistically insignificant towards the overall fit. And the average value of the squared deviations from the experimental values was minimized). The values of the virial coefficients a_0 to a_m were then used to calculate the isosteric heat of adsorption utilizing the following expression:

$$Q_{st} = -R \sum_{i=0}^{m} a_i N^i \qquad (3)$$

Q_{st} is the coverage-dependent isosteric heat of adsorption and R is the universal gas constant. The heat enthalpies of C_2H_2, CO_2 and C_2H_4 sorption for complex ZJU-280a in this manuscript are determined by using the sorption data measured in the pressure range from 0 to 1 bar (at 273 K and 296 K).

4. IAST calculations of adsorption selectivity

The selectivity of preferential adsorption of component A over component B in a mixture containing A and B, can be formally defined as:

$$S_{ads} = \frac{q_A / q_B}{p_A / p_B}$$

In equation (4), q_A and q_B are the molar loadings of the adsorbed phase in equilibrium with the bulk gas phase with partial pressures p_A and p_B.

5. Gas adsorption capacity and separation factor in experimental breakthrough tests

The complete breakthrough of C_2H_2 was indicated by downstream gas composition reaching that of feed gas. On the basis of the mass balance, gas adsorption capacities can be determined as follows:

$$q_i = \frac{C_i V}{22.4 \times m} \times \int_0^t (1 - \frac{F}{F_0})\, dt$$

Where q_i is the equilibrium adsorption capacity of gas component i (mmol g^{-1}), C_i is the feed gas concentration, V is the volumetric feed flow rate (mL min^{-1}), t is the adsorption time (min), F_0 and F are the inlet and outlet gas molar flow rates, respectively, and m is the mass of adsorbent (g). The separation factor (α) of the dynamic breakthrough experiments is determined as:

$$\alpha = \frac{q_1 / q_2}{y_1 / y_2}$$

where y_i is the molar fraction of gas i in the gas mixture.

6. Grand Canonical Monte Carlo simulations

In order to obtain reasonable binding sites of gas molecules in ZJU-280a for subsequent modeling, Grand Canonical Monte Carlo (GCMC) simulations were performed in the MS modeling. The crystal structure of ZJU-280a was chosen for related simulation without further geometry optimization. The framework and the individual C_2H_2, CO_2 and C_2H_4 molecules were considered to be rigid during the simulation. Partial charges for atoms of guest-free ZJU-280a were derived from QEq method and QEq_neutral1.0 parameter. The simulations were carried out at 298 K, adopting the locate task, Metropolis method in Sorption module and the universal force field (UFF). The partial charges on the atoms of C_2H_2 (C: -0.129e; H1: 0.129e, where e = 1.6022×10^{-19} C is the elementary charge), CO_2 (C: 0.894e; O: -0.447e) and C_2H_4 (C: -0.301e; H: 0.151e) were also derived from QEq method. The interaction energies between hydrocarbon molecules and framework were computed through the Coulomb and Lennard-Jones 6-12 (LJ) potentials. The cutoff radius was chosen as 12.5 Å for the LJ potential and the long-range electrostatic interactions were handled using the Ewald & Group summation method. The loading steps and the equilibration steps were 1×10^5, the production

steps were 1×10^6.

Notation

N	Adsorbed amount per mass of adsorbent i, mol kg^{-1}
b	Langmuir-Freundlich constant, kPa $^{-1/n_i}$
N^{max}	Saturation uptake for a specific site, mol kg^{-1}
n	Freundlich exponent, dimensionless
a_i	Virial coefficients, dimensionless
b_j	Virial coefficients, dimensionless
T	Absolute temperature, K
Q_{st}	Isosteric heat of adsorption, kJ mol^{-1}
q	Molar loading of the adsorbed species i, mol kg^{-1}

Greek letters

α	Separation factor, dimensionless

Scheme S1. Synthetic route to the organic linker of TPB.

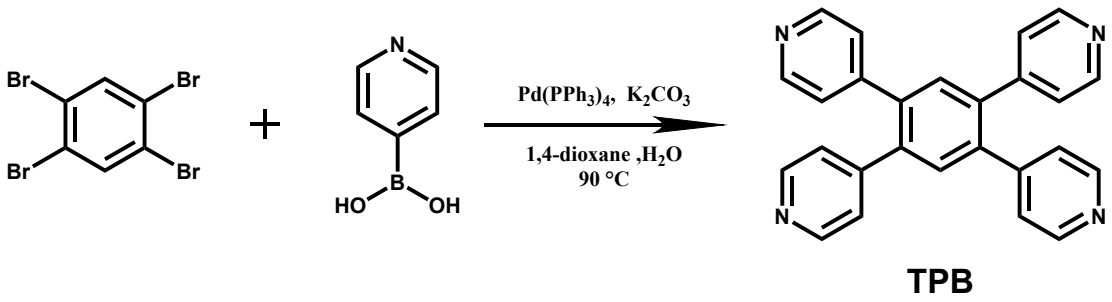

TPB

1,2,4,5-tetra(pyridin-4-yl) benzene (TPB). 1,2,4,5-tetrabromobenzene (7.48 g, 20 mmol), pyridin-4-ylboronic acid (14.8 g, 120 mmol), K_2CO_3 (44 g, 320 mmol), and $Pd(PPh_3)_4$ (800 mg, 0.692 mmol) were dissolved in 1,4-dioxane/H_2O (v/v = 3/1, 640 mL) under a dry N_2 atmosphere. And the mixture was stirred at 90 ℃ for two days. After the removal of 1,4-dioxane under reduced pressure, the reaction mixture was diluted with CH_2Cl_2, washed 4 times with brine, and dried over anhydrous $MgSO_4$. Then the precipitate was filtrated, while solvent was removed under vacuum. The crude product was purified by column chromatography (silica gel, dichloromethane/methanol, 25/1, v/v) to give white powder. Yield: 2.56 g (33%). ^{1}H NMR (500 MHz, Chloroform-d): δ 8.56 (m, 8H), 7.54 (s, 2H), 7.14 (m, 8H).

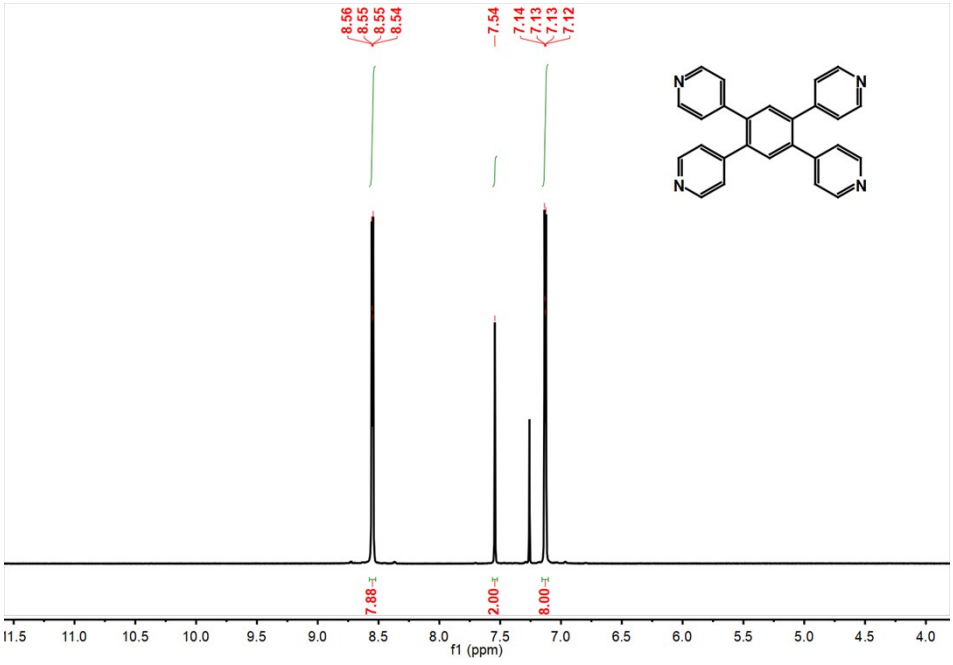

Figure S1. ^{1}H ($CDCl_3$, 500MHz) spectra of 1,2,4,5-tetra(pyridin-4-yl) benzene.

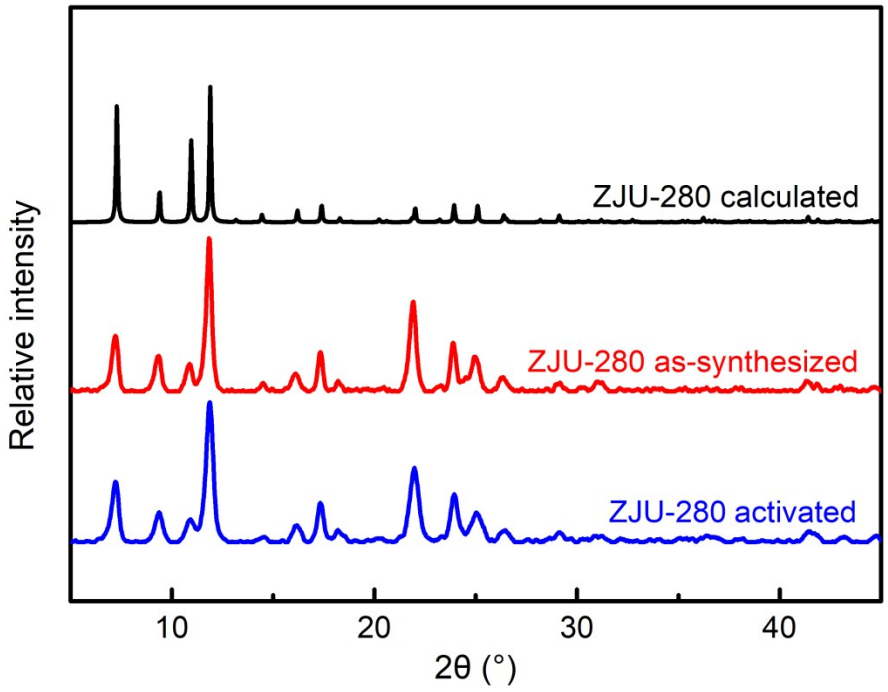

Figure S2. The calculated XRD pattern from the model structure of ZJU-280 (black) and PXRD patterns of as-synthesized ZJU-280 (red), activated ZJU-280a (blue). The simulated PXRD pattern of our structural model agrees excellently with the experimental data, strongly supporting its validity.

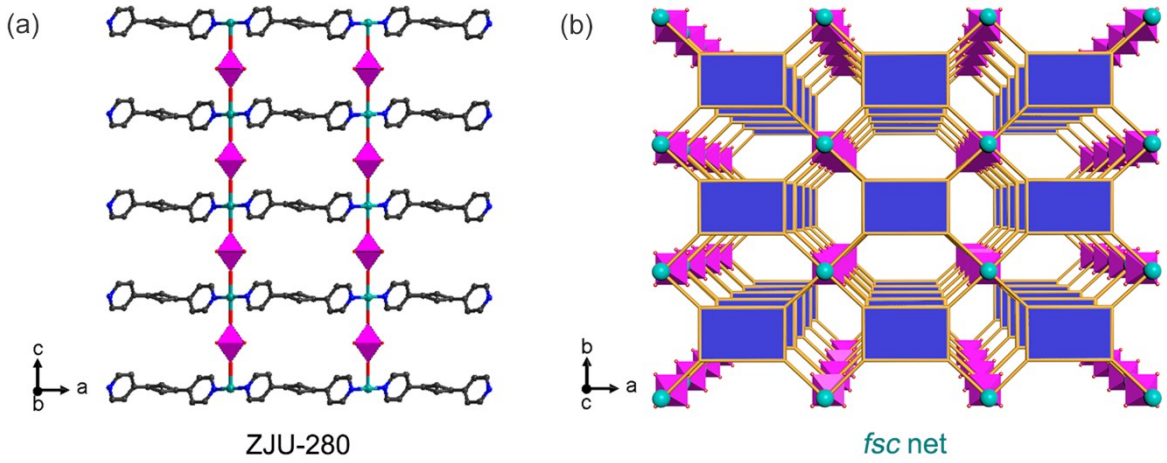

Figure S3. Structural description of ZJU-280. (a) Side view of ZJU-280a structure along the *b* axes; (b) top view of *fsc* topology along the *c* axes. Color code: Cu (cyan), Si (dark green), F (red), N (blue), and C (grey). H atoms are omitted for clarity.

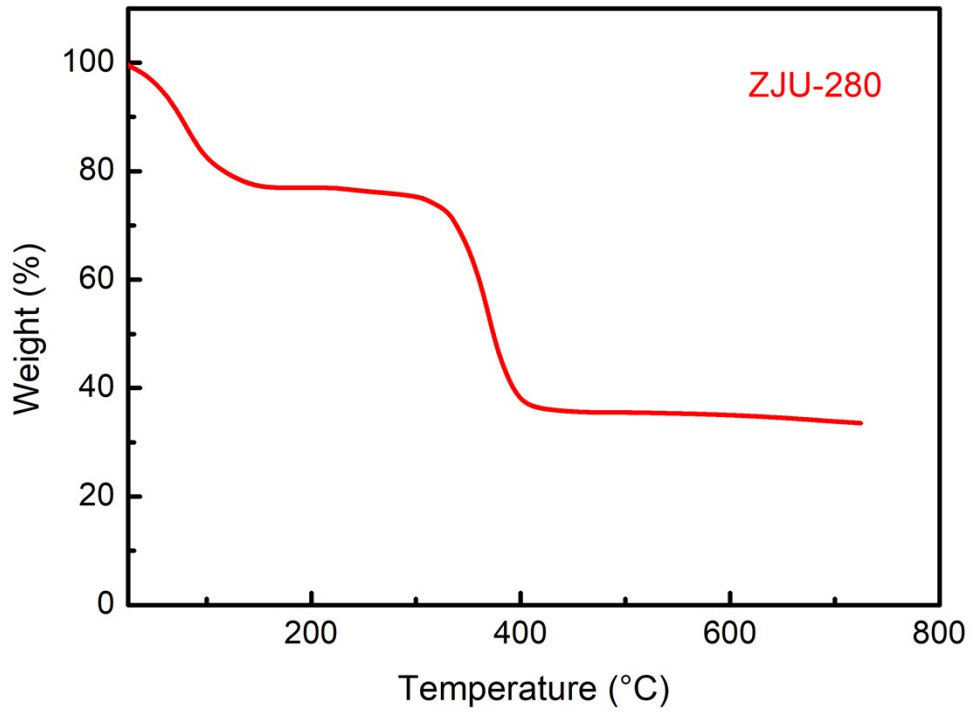

Figure S4. TGA curves of as-synthesized ZJU-280.

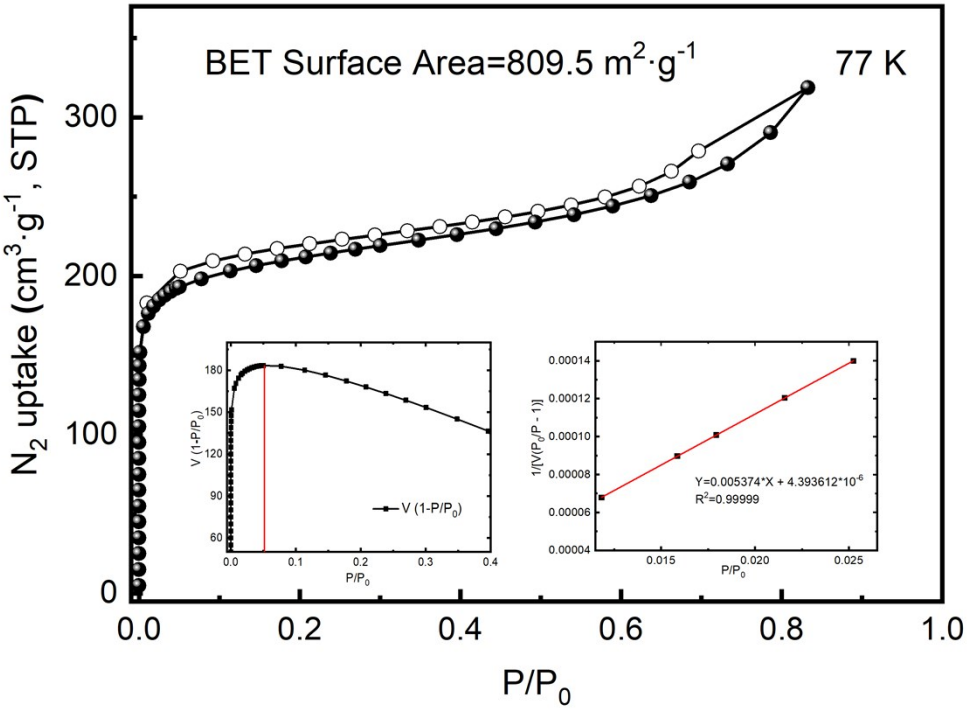

S_{BET} = (1/(0.005374+4.393612×10^{-6}))/22414×6.02×10^{23}×0.170×10^{-18}=809.5 m^2 g^{-1}

V_P = 0.49 cm^3 g^{-1}

Figure S5. N_2 sorption isotherms of ZJU-280a at 77 K. Filled/empty symbols represent adsorption/desorption.

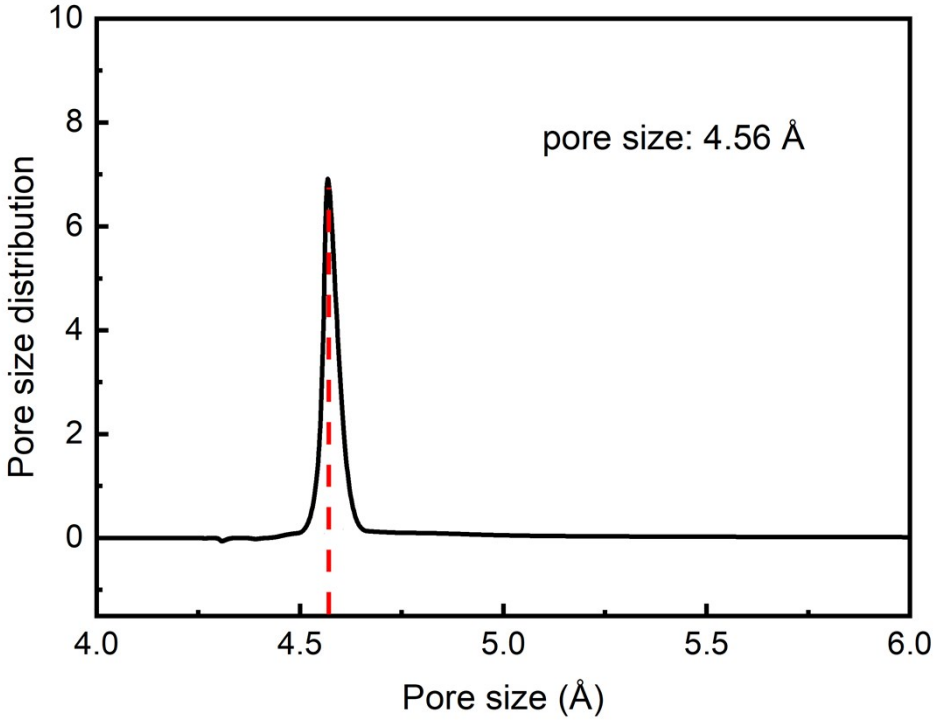

Figure S6. Pore size distribution for ZJU-280a based on Horvath-Kawazoe model.

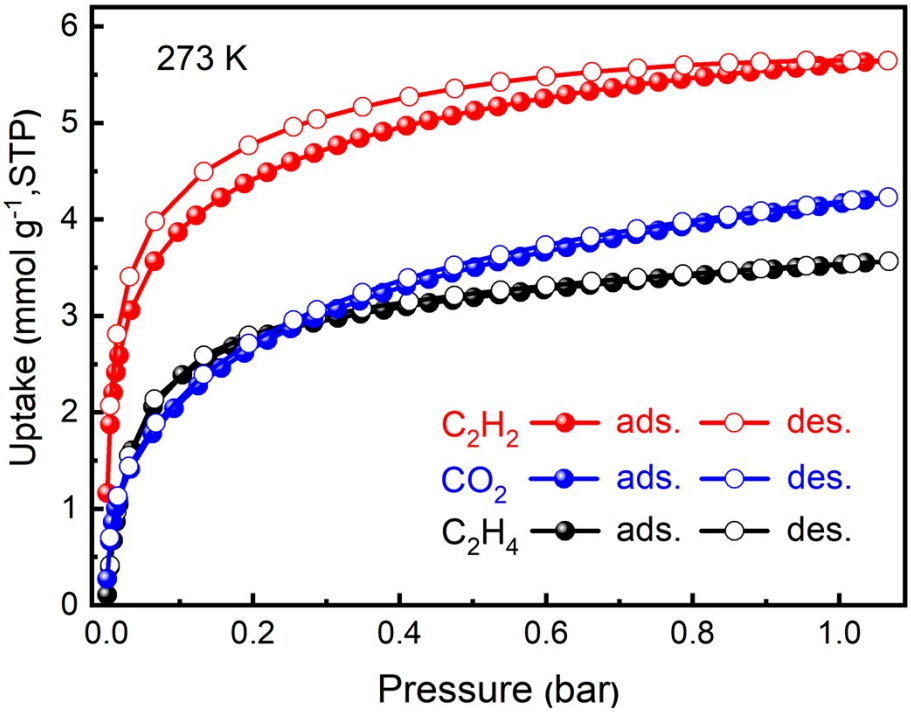

Figure S7. Adsorption isotherms of C_2H_2 (red), CO_2 (blue) and C_2H_4 (black) for ZJU-280a at 273 K up to 1 bar. Filled/empty symbols represent adsorption/desorption.

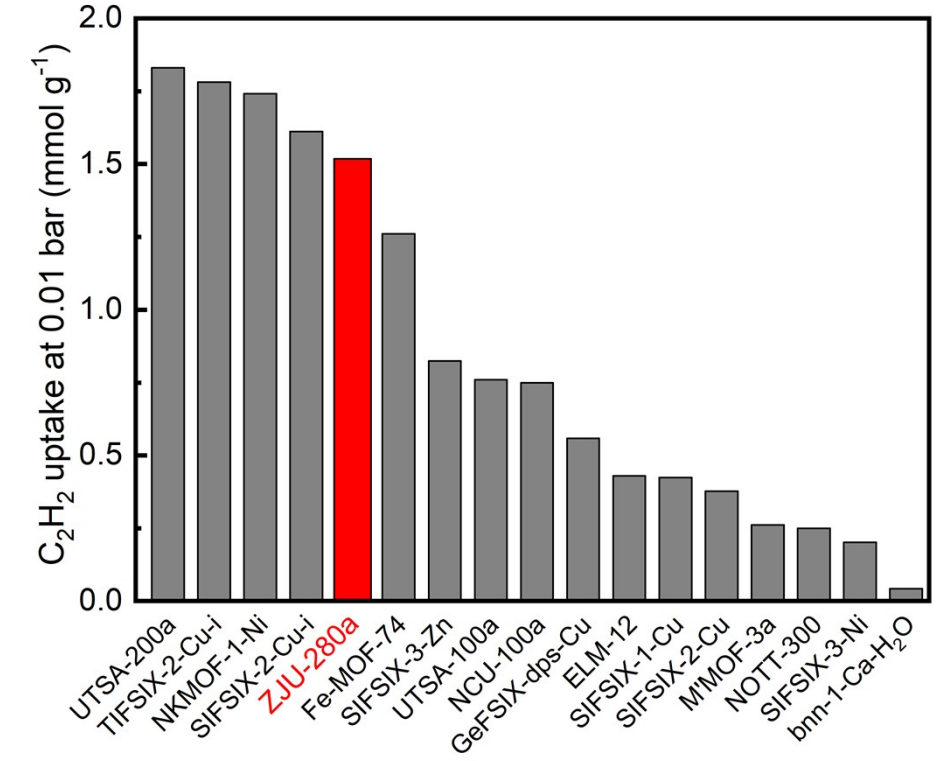

Figure S8. Comparison of the C_2H_2 uptake of ZJU-280a and other leading materials for C_2H_2/C_2H_4 separation at 0.01 bar and room temperature.

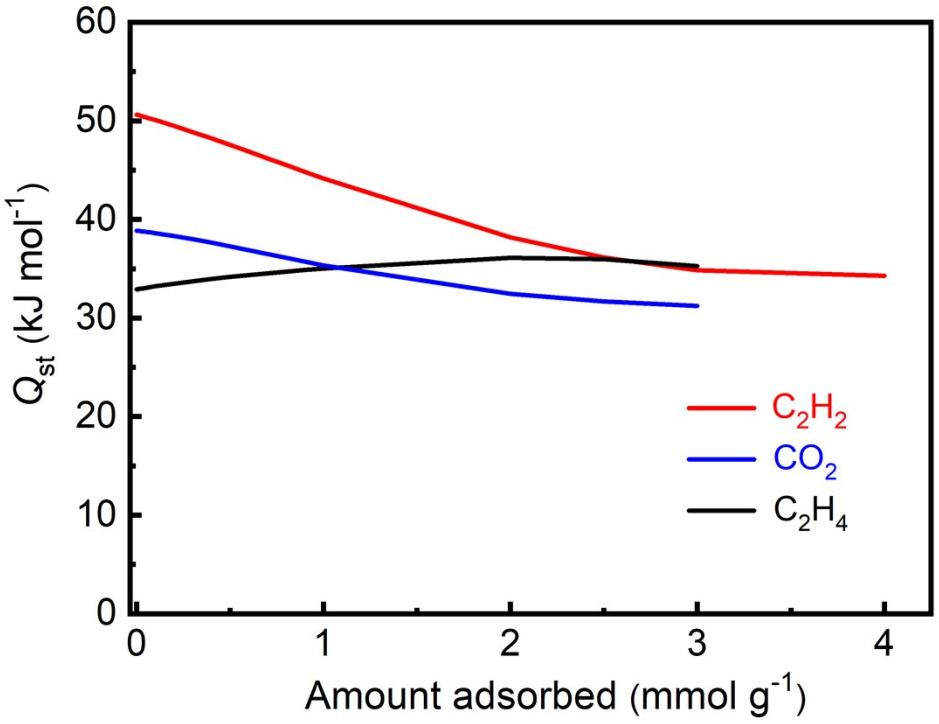

Figure S9. Heats of adsorption (Q_{st}) of C_2H_2 (red), CO_2 (blue) and C_2H_4 (black) for ZJU-280a.

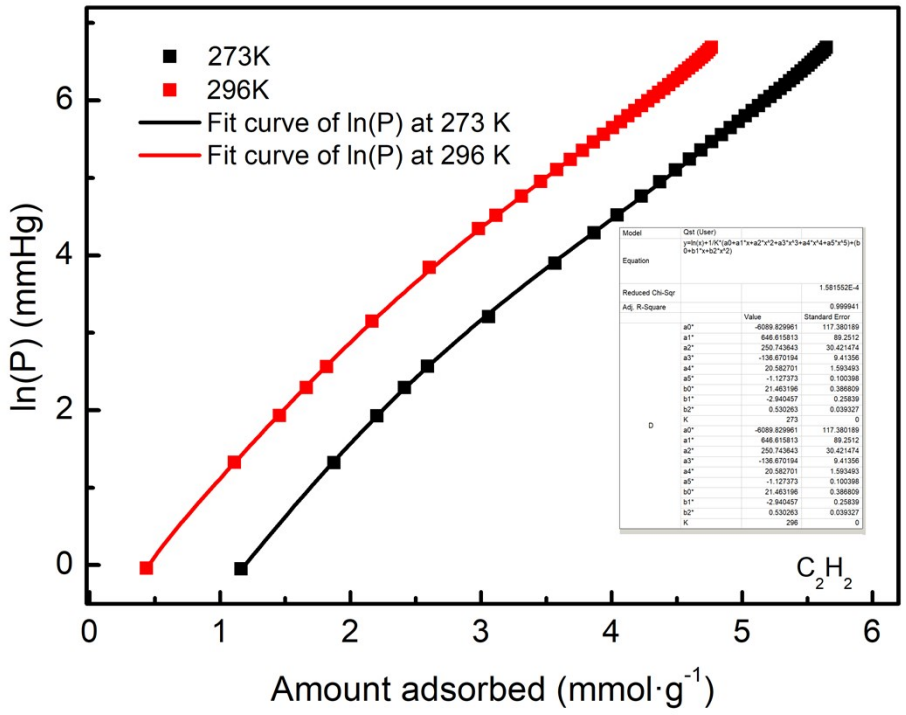

Figure S10. Virial fitting of the C_2H_2 adsorption isotherms for ZJU-280a.

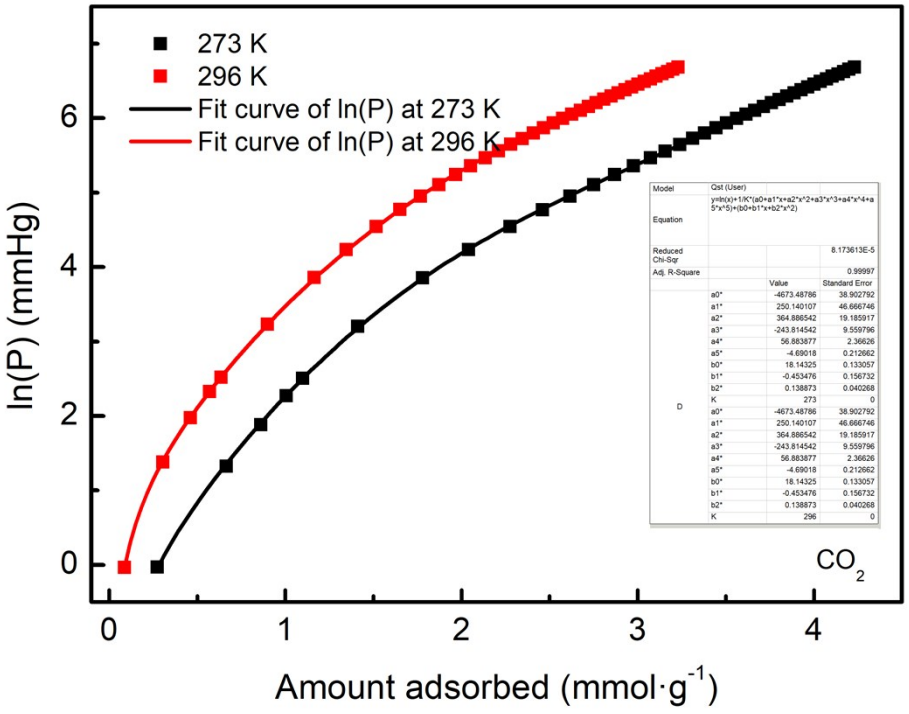

Figure S11. Virial fitting of the CO_2 adsorption isotherms for ZJU-280a.

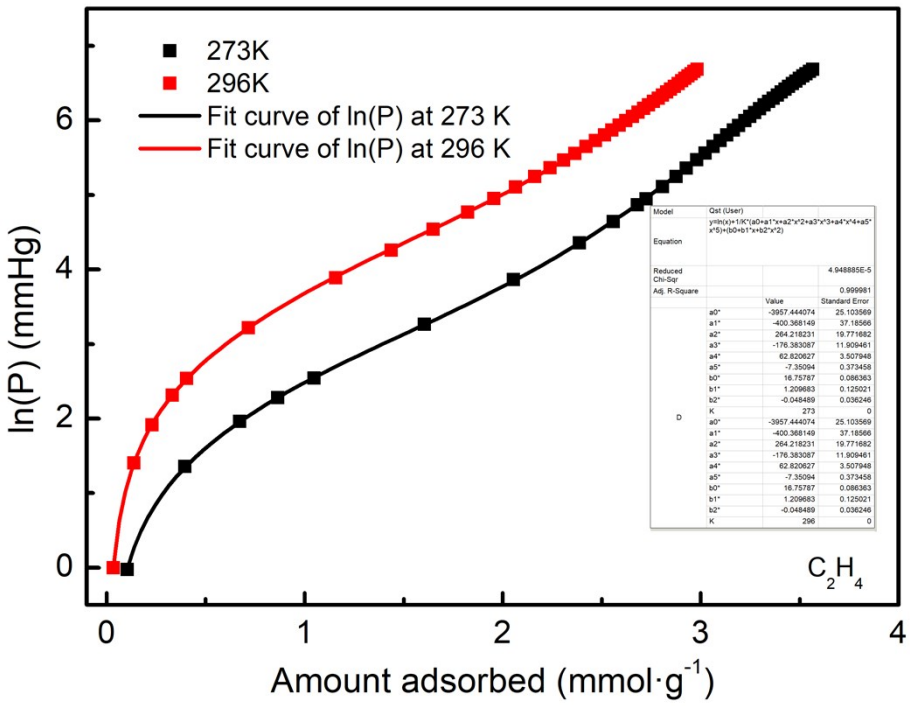

Figure S12. Virial fitting of the C_2H_4 adsorption isotherms for ZJU-280a.

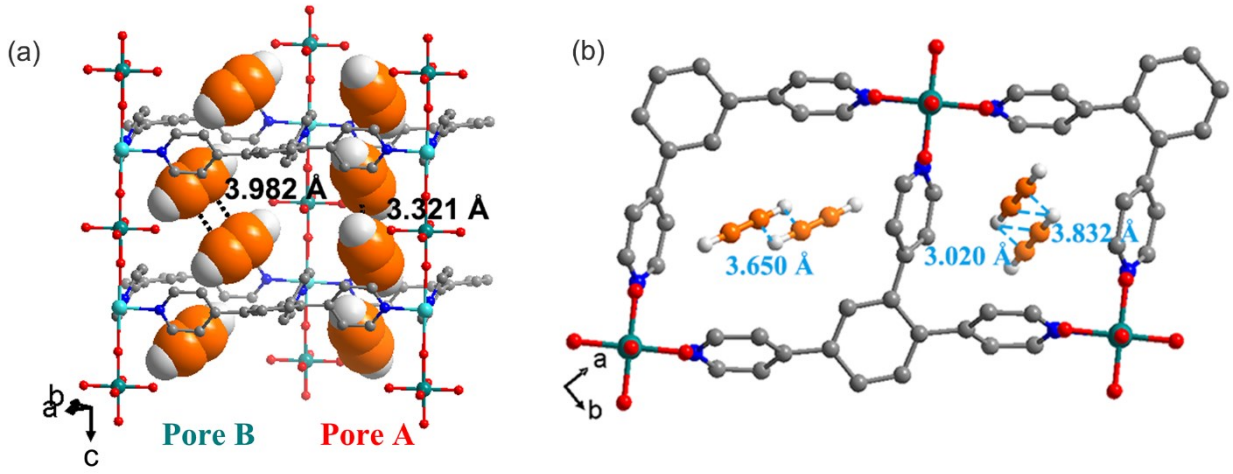

Figure S13. (a) Dense packing of C_2H_2 molecules within two pore channels of ZJU-280a and (b) the calculated C_2H_2 adsorption binding sites in the framework viewed along the *c* axes. Color code: Cu (cyan), Si (dark green), F (red), N (blue), H (white), and C (grey in ZJU-280a, orange in C_2H_2).

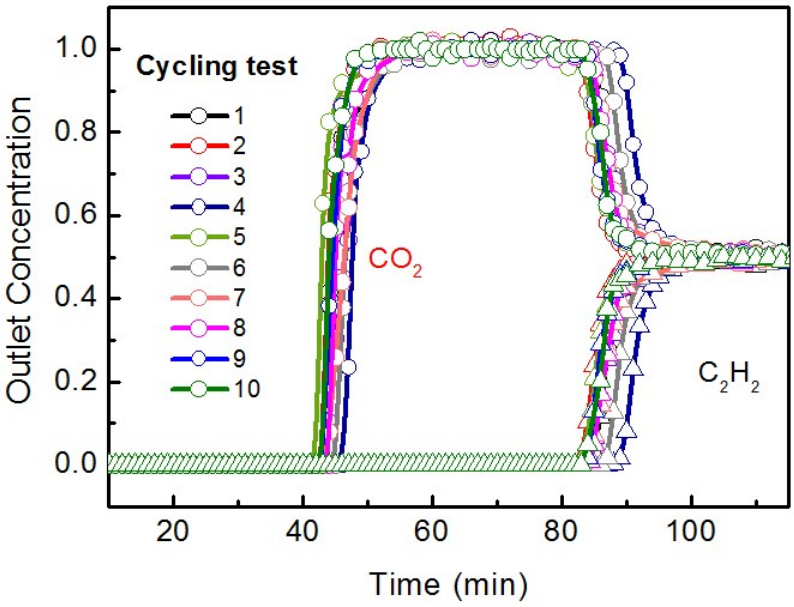

Figure S14. Multiple cycles of breakthrough tests of C_2H_2/CO_2 (50/50, v/v) gas mixtures with a total flow of 2 mL min^{-1} in an absorber bed packed with ZJU-280a at 298 K and 1 bar.

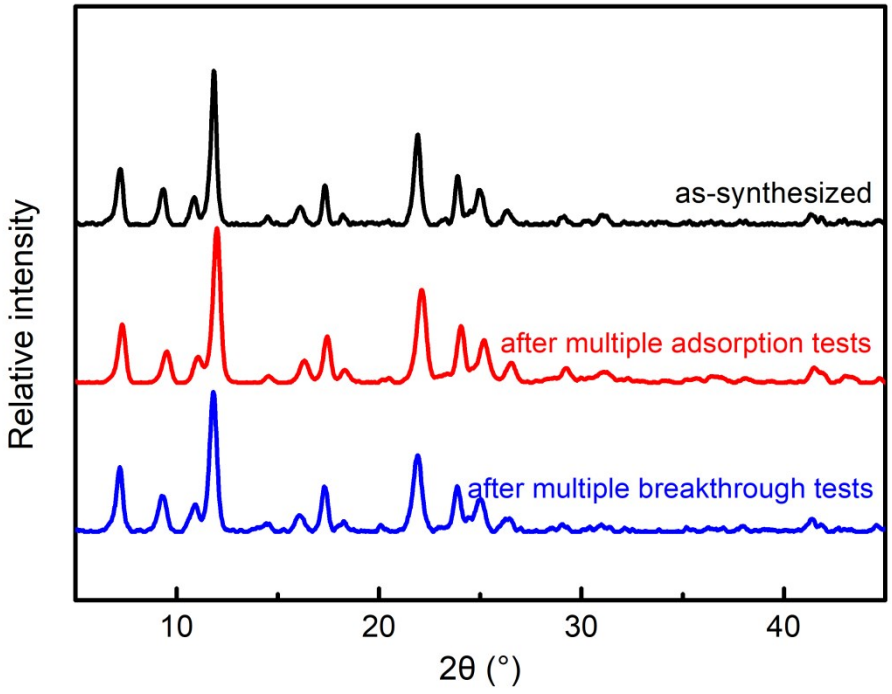

Figure S15. PXRD patterns of as-synthesized samples (black), the samples after the multiple adsorption tests (red), multiple breakthrough tests including experimental breakthrough for 50/50 C_2H_2/CO_2 in 60% humidity (blue) of ZJU-280a.

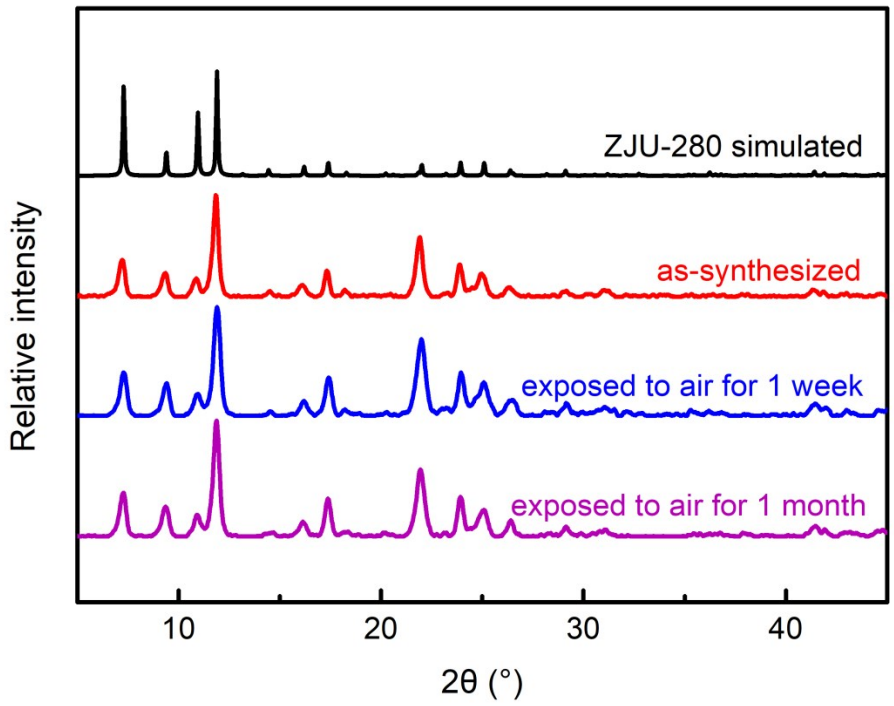

Figure S16. PXRD patterns of simulated (black), as-synthesized ZJU-280 (red), and ZJU-280 samples exposed to air for 1 week (blue) and 1 month (purple), indicating its great air stability.

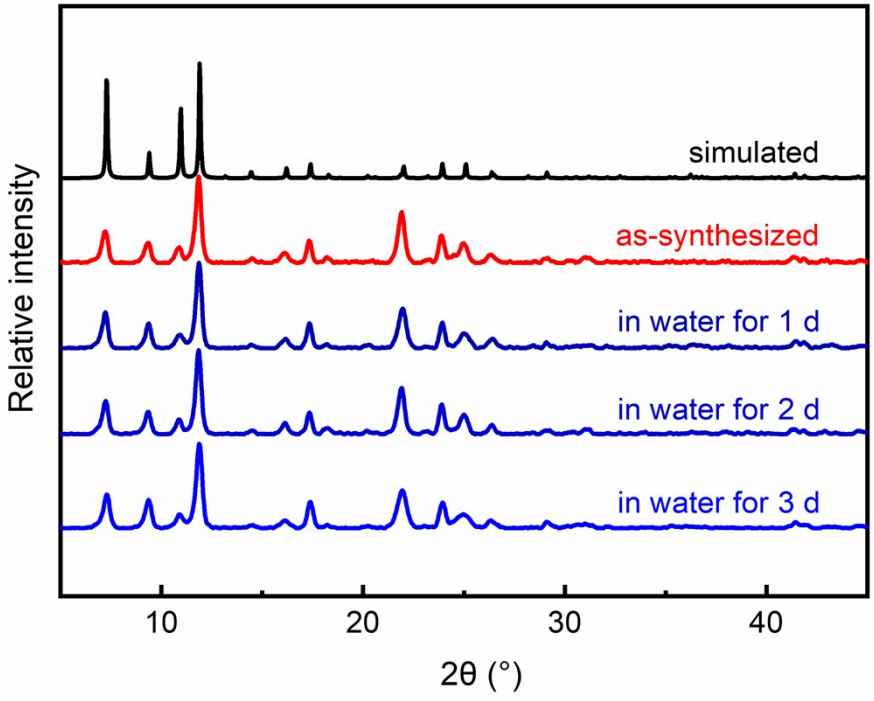

Figure S17. PXRD patterns of ZJU-280 after immersion in water for 1 day, 2 days and 3 days.

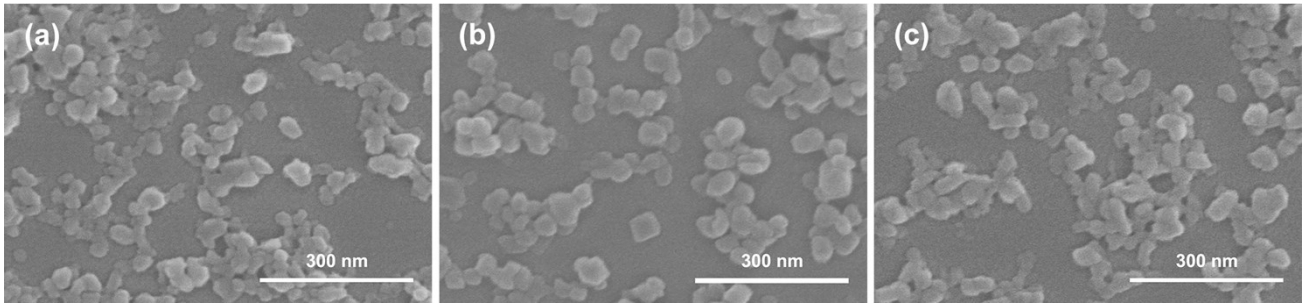

Figure S18. SEM images of (a) the as-synthesized sample, (b) the sample soaking in water for 3 days and (c) the sample after multiple breakthrough tests of ZJU-280a, indicating that the morphology and size/shape of the nanoparticles (ca. 50 nm) show almost unchanged after water treatment and separation experiments.

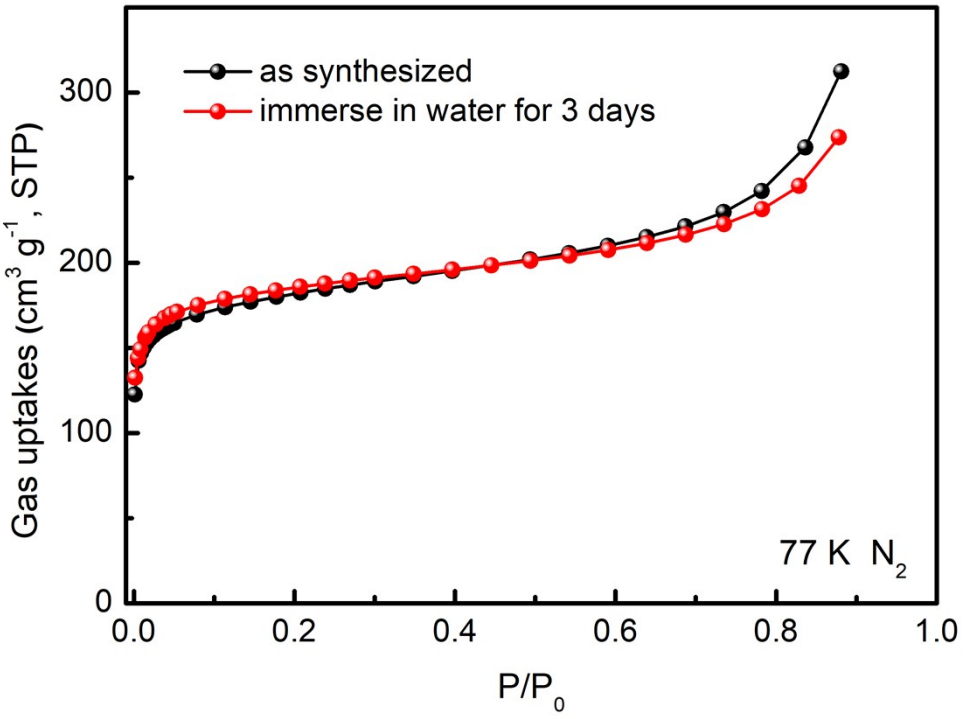

Figure S19. Comparison of N_2 adsorption isotherms at 77 K of ZJU-280a (black) and the re-activated sample after immersion in water for 3 days (red).

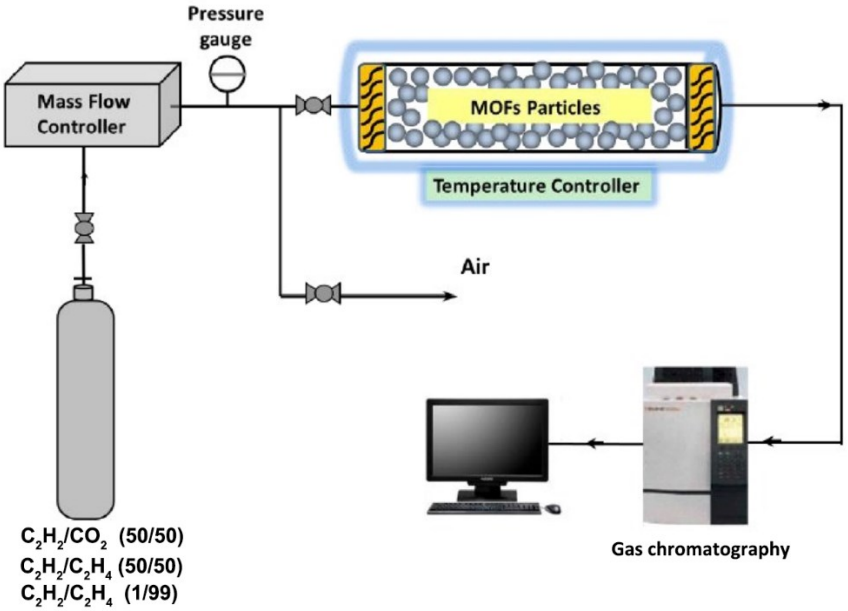

Breakthrough experiments apparatus

Figure S20. Schematic illustration of the apparatus for the breakthrough experiments.

Table S1. Lattice parameters of the modeled structure of ZJU-280.

Unit cell parameters	ZJU-280
Formula	$C_{26}H_{18}N_4F_6SiCu$
Formula weight	592.07
Crystal system	Monoclinic
Space group	*P*2/m
a (Å)	12.1200
b (Å)	9.4070
c (Å)	8.0690
α (°)	90.00
β (°)	90.00
γ (°)	90.00
V (Å^3)	919.97
Z	1
D_{calcd} (g cm^{-3})	1.069

Table S2. List of atomic coordinates for the modeled structure of ZJU-280.

Atoms	x	y	z	s.o.f.
C1	0.13981	0.23945	0.61965	1.00
C2	0.22588	0.33732	0.61597	1.00
C3	0.27626	0.24623	0.34810	1.00
C4	0.18639	0.15476	0.35714	1.00
C5	0.29762	0.33939	0.47957	1.00
C6	0.39896	0.42660	0.48252	1.00
H7	0.08849	0.22664	0.72966	1.00
H8	0.23950	0.40669	0.72230	1.00
H9	0.32863	0.24471	0.23816	1.00
H10	0.16550	0.08404	0.25512	1.00
N11	0.12043	0.15040	0.49174	1.00
F12	0.10220	0.13136	0.00064	1.00
C13	0.50000	0.35633	0.46404	1.00
H14	0.50000	0.24150	0.44367	1.00
F15	0.00000	-0.00562	0.21968	1.00
Cu16	0.00000	0.00000	0.50000	1.00
Si17	0.00000	0.00000	0.00000	1.00

Table S3. Dual-Langmuir-Freundlich parameter fits for C_2H_2, C_2H_4 and CO_2 in ZJU-280a. The fits are based on experimental isotherm data at 296 K.

	Site Ⅰ			Site Ⅱ		
	N_1^{max} mol kg^{-1}	b_1 kPa$^{-1/n_1}$	$1/n_1$ dimensionless	N_2^{max} mol kg^{-1}	b_2 kPa$^{-1/n_2}$	$1/n_2$ dimensionless
C_2H_2	3.81511	0.12167	0.65019	2.85119	0.6934	0.2748
C_2H_4	2.26328	0.09787	1.1021	1.88796	0.02469	0.74738
CO_2	5.07516	0.0235	0.76252	0.95467	0.60451	0.88342

Table S4. Comparison of the gas uptake and selectivity of ZJU-280a with some top-performing MOFs reported for C_2H_2/CO_2 (50/50, v/v) separation.

MOF	Uptake ($cm^3\ g^{-1}$)	IAST selectivity	Q_{st}[b] (kJ mol^{-1})		Ref.
	C_2H_2 at 0.5 bar	C_2H_2/CO_2[a] (50/50, v/v)	C_2H_2	CO_2	
ZJU-280a	94.9	18.1	50.6	38.8	This work
FeNi-M'MOF	91.1	24	27	24.5	3
NKMOF-1-Ni	55.5	22	60.3	40.9	4
HOF-3a	42.5	21	19	42	5
BSF-3	69.6	16.3	42.7	22.4	6
DICRO-4-Ni-i	36.3	13.9	37.7	33.9	7
JCM-1	63.5	13.7	36.9	33.4	8
UTSA-74a	88.9	9	31	25	9
SIFSIX-3-Ni	65.7	Inverse 7.7[c]	36.7	50.9	10
TIFSIX-2-Cu-i	83	6.5[c]	46.3	35.8	10
MUF-17	62.9	6	49.5	33.8	11
PCP-33	89	6	27.5	26.2	12
CPM-107	74.1	5.7	37	24	13
SNNU-45	114.1	4.5	39.9	27.1	14
FJU-90a	154.5	4.3	25.1	20.7	15
JNU-1	53	3.6	47.6[d]	-	16
UPC-200(Al)-F-BIM	75.8	3.2	18.9-20.5	-	17
FJU-6-TATB	69.7	3.1	29	26	18
Zn-MOF-74	102	1.9	24	-	19

[a] A total pressure of 1 bar.

[b] Q_{st} values at low surface coverage.

[c] IAST selectivity for C_2H_2/CO_2 (2/1, v/v) gas mixtures.

[d] The maximum Q_{st} value.

Table S5. Comparison of C_2H_2/CO_2 selectivity and C_2H_2/C_2H_4 selectivity for ZJU-280a with the reported materials that are capable of both C_2H_2/CO_2 and C_2H_2/C_2H_4 separation.

MOF	Uptake ($cm^3\ g^{-1}$)		IAST Selectivity			Q_{st}[b] ($kJ\ mol^{-1}$)	Ref.
	C_2H_2 at 0.01 bar	C_2H_2 at 0.5 bar	C_2H_2/CO_2[a] (50/50, v/v)	C_2H_2/C_2H_4[a] (1/99, v/v)	C_2H_2/C_2H_4[a] (50/50, v/v)	C_2H_2	
ZJU-280a	34	94.8	18.1	44.5	33	50.6	This work
NKMOF-1-Ni	39	55.5	22	44	-	60.3	4
BSF-3	16.6	69.6	16.3	-	8	42.7	6
pacs-CoMOF-2a	24.7	107.1	13	11.5	-	34.2	20
BSF-3-Co	16	77.4	12.7	-	10.7	-	6
JCM-1	10.1	63.5	13.7	8.1	13.2	36.9	8
BSF-4	11.8	45.1	9.8	-	7.3	35	21
SIFSIX-3-Ni	4.5	65.7	Inverse 7.7[c]	5	6	36.7	10
TIFSIX-2-Cu-i	39.9	83	6.5[c]	55	-	46.3	10
ZU-12-Ni	25.8	84.1	6.2[c]	22.7	-	40	22
MUF-17	31.2	62.9	6	7.1	8.7	49.5	11
PCP-33	-	89	6	-	2	27.5	12
BSF-2	3.3	33.4	5.1	-	2.9	37.3	6
UTSA-220	22.6	70.2	4.4	10	8.8	29	1c
HUST-6	8.6	52.6	3.4[d]	-	2.4[d]	31.1	23
BSF-1	2.2	35.3	3.3	-	2.3	31	24
FJU-22a	43.9	106.5	-	-	-	23	25
SIFSIX-1-Cu	9.5	171.6	-	10.6	8.4	30	26
SIFSIX-2-Cu-i	36.1	82.8	-	44.8	41	53	26
UTSA-100a	17.1	81.4	-	10.7	19.4	22	27
UTSA-200a	41	76.4	-	6320	-	56	28

[a] A total pressure of 1 bar and room temperature.

[b] At low loading.

[c] IAST selectivity for C_2H_2/CO_2 (2/1, v/v) gas mixtures.

[d] At 273 K.

Disclaimer: Certain commercial suppliers are identified in this paper to foster understanding. Such identification does not imply recommendation or endorsement by the National Institute of Standards and Technology, nor does it imply that the materials or equipment identified are necessarily the best available for the purpose.

References

[1] (*a*) H.-M. Wen, L. Li, R.-B. Lin, B. Li, B. Hu, W. Zhou, J. Hu and B. Chen, *J. Mater. Chem. A*, 2018, **6**, 6931; (*b*) G. Xu, B. Li, H. Wu, W. Zhou and B. Chen, *Cryst. Growth Des.*, 2017, **17**, 4795; (*c*) H. Li, L. Li, R.-B. Lin, G. Ramirez, W. Zhou, R. Krishna, Z. Zhang, S. Xiang and B. Chen, *ACS Sustainable Chem. Eng.*, 2019, **7**, 4897.

[2] Q. Lin, C. Mao, A. Kong, X. Bu, X. Zhao and P. Feng, *J. Mater. Chem. A*, 2017, **5**, 21189.

[3] J. Gao, X. Qian, R.-B. Lin, R. Krishna, H. Wu, W. Zhou and B. Chen, *Angew. Chem., Int. Ed.*, 2020, **59**, 4396.

[4] Y.-L. Peng, T. Pham, P. Li, T. Wang, Y. Chen, K.-J. Chen, K. A. Forrest, B. Space, P. Cheng, M. J. Zaworotko and Z. Zhang, *Angew. Chem., Int. Ed.*, 2018, **57**, 10971.

[5] P. Li, Y. He, Y. Zhao, L. Weng, H. Wang, R. Krishna, H. Wu, W. Zhou, M. O'Keeffe, Y. Han and B. Chen, *Angew. Chem., Int. Ed.*, 2015, **54**, 574.

[6] Y. Zhang, J. Hu, R. Krishna, L. Wang, L. Yang, X. Cui, S. Duttwyler and H. Xing, *Angew. Chem., Int. Ed.*, 2020, **59**, 17664.

[7] H. S. Scott, M. Shivanna, A. Bajpai, D. G. Madden, K.-J. Chen, T. Pham, K. A. Forrest, A. Hogan, B. Space, J. J. Perry Ⅳ and M. J. Zaworotko, *ACS Appl. Mater. Interfaces*, 2017, **9**, 33395.

[8] J. Lee, C. Y. Chuah, J. Kim, Y. Kim, N. Ko, Y. Seo, K. Kim, T. H. Bae and E. Lee, *Angew. Chem., Int. Ed.*, 2018, **57**, 7869.

[9] F. Luo, C. Yan, L. Dang, R. Krishna, W. Zhou, H. Wu, X. Dong, Y. Han, T.-L. Hu, M. O'Keeffe, L. Wang, M. Luo, R.-B. Lin and B. Chen, *J. Am. Chem. Soc.*, 2016, **138**, 5678.

[10] K.-J. Chen, H. S. Scott, D. G. Madden, T. Pham, A. Kumar, A. Bajpai, M. Lusi, K. A. Forrest, B. Space, J. J. Perry Ⅳ and M. J. Zaworotko, *Chem*, 2016, **1**, 753.

[11] O. T. Qazvini, R. Babarao and S. G. Telfer, *Chem. Mater.*, 2019, **31**, 4919.

[12] J. Duan, W. Jin and R. Krishna, *Inorg. Chem.*, 2015, **54**, 4279.

[13] H. Yang, T. X. Trieu, X. Zhao, Y. Wang, Y. Wang, P. Feng and X. Bu, *Angew. Chem., Int. Ed.*, 2019, **58**, 11757.

[14] Y.-P. Li, Y. Wang, Y.-Y. Xue, H.-P. Li, Q.-G. Zhai, S.-N. Li, Y.-C. Jiang, M.-C. Hu and X. Bu, *Angew. Chem., Int. Ed.*, 2019, **58**, 13590.

[15] Y. Ye, Z. Ma, R.-B. Lin, R. Krishna, W. Zhou, Q. Lin, Z. Zhang, S. Xiang and B. Chen, *J. Am. Chem. Soc.*, 2019, **141**, 4130.

[16] H. Zeng, M. Xie, Y.-L. Huang, Y. Zhao, X.-J. Xie, J.-P. Bai, M.-Y. Wan, R. Krishna, W. Lu and D. Li, *Angew. Chem., Int. Ed.*, 2019, **58**, 8515.

[17] W. Fan, S. Yuan, W. Wang, L. Feng, X. Liu, X. Zhang, X. Wang, Z. Kang, F. Dai, D. Yuan, D. Sun and H.-C. Zhou, *J. Am. Chem. Soc.*, 2020, **142**, 8728.

[18] L. Liu, Z. Yao, Y. Ye, Y. Yang, Q. Lin, Z. Zhang, M. O'Keeffe and S. Xiang, *J. Am. Chem. Soc.*, 2020, **142**, 9258.

[19] S. Xiang, W. Zhou, Z. Zhang, M. A. Green, Y. Liu and B. Chen, *Angew. Chem., Int. Ed.*, 2010, **49**, 4615.

[20] D.-M. Chen, C.-X. Sun, N.-N. Zhang, H.-H. Si, C.-S. Liu and M. Du, *Inorg. Chem.*, 2018, **57**, 2883.

[21] Y. Zhang, L. Wang, J. Hu, S. Duttwyler, X. Cui and H. Xing, *CrystEngComm*, 2020, **22**, 2649.

[22] M. Jiang, X. Cui, L. Yang, Q. Yang, Z. Zhang, Y. Yang and H. Xing, *Chem. Eng. J.*, 2018, **352**, 803.

[23] F. Yu, B.-Q. Hu, X.-N. Wang, Y.-M. Zhao, J.-L. Li, B. Li and H.-C. Zhou, *J. Mater. Chem. A*, 2020, **8**, 2083.

[24] Y. Zhang, L. Yang, L. Wang, S. Duttwyler and H. Xing, *Angew. Chem., Int. Ed.*, 2019, **58**, 8145.

[25] Z. Yao, Z. Zhang, L. Liu, Z. Li, W. Zhou, Y. Zhao, Y. Han, B. Chen, R. Krishna and S. Xiang, *Chem. Eur. J.*, 2016, **22**, 5676.

[26] (*a*) X. Cui, K. Chen, H. Xing, Q. Yang, R. Krishna, Z. Bao, H. Wu, W. Zhou, X. Dong, Y. Han, B. Li, Q. Ren, M. J. Zaworotko and B. Chen, *Science*, 2016, **353**, 141. (*b*) A. Bajpai, D. O'Nolan, D. G. Madden, K.-J. Chen, T. Pham, A. Kumar, M. Lusi, J. J. Perry, B. Space and M. J. Zaworotko, *Chem. Commun.*, 2017, **53**, 11592.

[27] T.-L. Hu, H. Wang, B. Li, R. Krishna, H. Wu, W. Zhou, Y. Zhao, Y. Han, X. Wang, W. Zhu, Z. Yao, S. Xiang and B. Chen, *Nat. Commun.*, 2015, **6**, 7328.

[28] B. Li, X. Cui, D. O'Nolan, H.-M. Wen, M. Jiang, R. Krishna, H. Wu, R.-B. Lin, Y.-S. Chen, D. Yuan, H. Xing, W. Zhou, Q. Ren, G. Qian, M. J. Zaworotko and B. Chen, *Adv. Mater.*, 2017, **29**, 1704210.